Explicit Matrix-Free Time-Domain Method in Unstructured Meshes and Its Application to Stable Simulation of General Unsymmetrical Systems

Kaiyuan Zeng, *Member, IEEE*, and Dan Jiao, *Fellow, IEEE*

***Abstract*— The existing matrix-free time-domain (MFTD) method, though free of a matrix solution in arbitrary unstructured meshes, is not explicit in time marching, as a backward difference is utilized. The numerical system underlying the MFTD is unsymmetrical, and a traditional explicit simulation of such a system is absolutely unstable. In this article, we overcome this barrier and successfully develop a truly explicit MFTD method. In this method, a new explicit time marching scheme is created for simulating unsymmetrical systems, whose stability is theoretically proved and shown to be guaranteed. Meanwhile, the accuracy is not sacrificed; and the time step allowed by the traditional explicit method is not reduced to ensure the stability. As a result, we greatly improve the computational efficiency of the MFTD method without compromising its accuracy. In addition to the MFTD, the unsymmetrical systems are encountered in other numerical methods and analyses, such as the subgridding methods, the nonorthogonal FDTD methods, and the analysis of nonreciprocal problems. In this article, we show that the proposed new explicit method is a general method for stably simulating unsymmetrical systems. Hence, it can be utilized in other unsymmetrical methods to ensure the stability in an explicit time-domain simulation. The accuracy, efficiency, and stability of the proposed work have been demonstrated by extensive numerical experiments.**

***Index Terms*— Explicit time marching, finite-difference time-domain (FDTD) method, matrix-free methods, stability, subgridding, time-domain methods, unstructured mesh, unsymmetrical system.**

I. Introduction

AMONG the existing time-domain computational electromagnetic methods, the explicit finite-difference time-domain (FDTD) method [1], [2] requires a structured orthogonal grid for space discretization. The finite-element method in time domain (TDFEM) [3], [9], [10] has no difficulty in handling arbitrarily shaped irregular meshes, but it requires the solution of a mass matrix even in its explicit schemes. Recently, a matrix-free time-domain (MFTD) method is developed for solving Maxwell's equations and other partial differential equations (PDEs) in unstructured meshes [11]–[14]. It possesses the advantages of both the FDTD and the TDFEM: having a naturally diagonal mass matrix, which is achieved accurately, and also independent of the element shape used for space discretization. However, the underlying discretized curl–curl operator is highly unsymmetrical. For an unsymmetrical matrix, a traditional leap-frog or central-difference-based explicit time marching is absolutely unstable, a proof of which can be found in [11], [13], and [24]. This is because an unsymmetrical matrix can support complex eigenvalues or even negative eigenvalues; when these eigenvalues exist, no time step can be found to make the explicit time marching stable. To overcome the stability problem while retaining the advantage of a diagonal mass matrix, in [11]–[13], a backward difference scheme is employed for time marching. This results in a system matrix to solve, which is an implicit scheme. Although the inverse of the system matrix is made explicit in [11]–[13] by using a series expansion, thus avoiding a matrix solution, the computation of a k-term series expansion is still required, which is equivalent to k sparse matrix-vector multiplications. The value of k is small, and however, the computational cost is higher than a true explicit scheme, which requires only one matrix-vector multiplication.

The unsymmetrical numerical systems are also commonly encountered in other numerical methods, such as nonorthogonal FDTD methods [8], [24], FDTD subgridding schemes [4]–[7], [25]–[28], and FDTD with nonuniform gridding. In an FDTD subgridding scheme, the fields at the interface between a base grid and a subgrid are typically obtained by an interpolation scheme using surrounding fields. To ensure the accuracy, such an interpolation scheme often results in an unsymmetrical numerical system, whose stability is not guaranteed. To ensure stability, the reciprocity of the fields has been enforced [25]–[27]. However, it is difficult to preserve the symmetry of the original FDTD without compromising accuracy and meshing flexibility. In a recent FDTD subgridding method [28], an accurate interpolation scheme is

Manuscript received May 3, 2019; revised September 14, 2019; accepted October 25, 2019. Date of publication December 13, 2019; date of current version December 27, 2019. This work was supported in part by the NSF under Award 1619062 and in part by the Defense Advanced Research Projects Agency (DARPA) under Award FA8650-18-2-7847. This article is an expanded version from the IEEE MTT-S International Microwave Symposium (IMS 2019), Boston, MA, USA, June 2–7, 2019. *(Corresponding author: Dan Jiao.)*

The authors are with the School of Electrical and Computer Engineering, Purdue University, West Lafayette, IN 47907 USA (e-mail: djiao@purdue.edu).

Color versions of one or more of the figures in this article are available online at http://ieeexplore.ieee.org.

Digital Object Identifier 10.1109/TMTT.2019.2951669

developed to ensure the accuracy of the resulting subgridding algorithm, and this scheme is applicable to arbitrary grid ratios between the base grid and the subgrid, as well as allowing for flexible subgrid arrangements and nonuniform gridding. However, the resultant system matrix is also unsymmetrical. As can be seen from [28], a special implicit scheme such as the one in [11] is used to address the stability.

Various nonorthogonal FDTD methods [8], [15]–[22] have also been developed to extend the capability of a standard FDTD to handle irregular meshes. In unstructured meshes, since the **H** loop cannot center the **E**-unknown and vice versa, interpolation and projection are often employed in the nonorthogonal FDTD methods to discretize Maxwell's equations. The resultant numerical system is, in general, unsymmetrical, and late time instability has been reported [23].

The stability and accuracy of the aforementioned methods have always been two competing factors. In order to ensure the accuracy of these methods, the resultant system matrix, in general, cannot be made symmetric. As a result, there is no theoretical guarantee of the stability of the resultant time-domain simulation. If the imaginary part of the eigenvalues of the unsymmetrical system matrix is negligible compared with the real part, such as a subgridding with a few interface unknowns or nonuniform gridding in small local areas, an explicit time marching may manage to be stable within a certain time window. However, this is not the case when the system matrix is highly unsymmetrical. For example, in the MFTD, we observe an immediate divergence after starting the time marching if a traditional explicit scheme is used. On the other hand, one can construct a symmetric numerical system to guarantee stability, however, accuracy and flexibility are often sacrificed in the space discretization of the curl operators. If we can find a systematic way to handle complex-valued eigenvalues and explicitly simulate an unsymmetrical numerical system with guaranteed stability, then not only the MFTD method can be made truly explicit, but also other unsymmetrical time-domain methods can be marched on in time explicitly without the need for concerning about their stability. When analyzing the problems that are unsymmetrical in nature such as nonreciprocal problems, being able to stably simulate unsymmetrical problems becomes even more critical.

The contribution of this article is such a method to overcome the instability of explicitly simulating an unsymmetrical numerical system. With this method, we are able to make the MFTD truly explicit, hence removing the need for using the backward difference and the series expansion to avoid a matrix solution. As a result, the advantage of the diagonal mass matrix of the MFTD is accentuated, and the matrix-free merit is strictly realized for unstructured meshes. The basic idea of this article has been presented in our conference article [30]. In this article, we provide a rigorous theoretical proof on the stability of the proposed method in addition to an accuracy analysis. We also extend the work to other unsymmetrical methods. A state-of-the-art unsymmetrical FDTD subgridding method [28] is made explicit without sacrificing accuracy using the proposed method. In addition, we have performed extensive numerical experiments on the new explicit unsymmetrical FDTD subgridding algorithm and the explicit MFTD method using various examples. They demonstrate the stability of the proposed explicit method in simulating unsymmetrical systems, with greatly reduced CPU run time and without sacrificing accuracy.

II. Background and Analysis of the Problem

In this section, we provide the background of this article and also analyze the problem encountered in the transient simulation of an unsymmetrical numerical system. We start from the MFTD in unstructured meshes, then proceed to the state-of-the-art unsymmetrical FDTD subgridding method, and then to the general unsymmetrical methods for solving Maxwell's equations.

A. MFTD in Unstructured Meshes and Underlying Unsymmetrical System

Given an irregular structure with inhomogeneous materials discretized into an arbitrary unstructured mesh, based on [11]–[13], the electric field **E** in each element is expanded into vector bases whose order is no less than one, such that the resulting curl **E** is not a constant in the element. As a result, the **H** field's space dependence in a single element can be captured, as its order would be higher than zero. If the traditional zeroth-order bases are used to represent **E** such as those in the FDTD, after taking a curl operation on **E**, the resulting magnetic field **H** is a constant in each element. As a result, **H** required for reversely finding **E** at the next time step cannot be accurately obtained in an irregular mesh.

The expansion into vector bases yields $\mathbf{E} = \sum_{j=1}^{m} e_j \mathbf{N}_j$, where e_j is the jth basis's unknown coefficient and m is the basis number in each element. Using the modified higher order vector bases shown in [11], each e_j denotes $\mathbf{E}(\mathbf{r}_{ej}) \cdot \hat{e}_j$, i.e., **E** field at point $\mathbf{r}_{ei}$ along the direction of unit vector $\hat{e}_j$. Substituting the expansion of **E** into Faraday's law, evaluating **H** at a point $\mathbf{r}_{hi}$, and then taking the dot product of the resultant with a unit vector $\hat{h}_i$, we obtain

$$-\text{diag}(\{\mu\})\frac{\partial\{h\}}{\partial t} = \mathbf{S}_e\{e\} \tag{1}$$

where $\{e\}$ denotes a global **E**-unknown vector of length N_e consisting of all e_j coefficients, $\mathbf{S}_e$ is a sparse matrix denoting a discretized curl operation on **E**, and h is a global **H**-unknown vector of length N_h, whose ith entry is $h_i = \mathbf{H}(\mathbf{r}_{hi}) \cdot \hat{h}_i$. The diag($\{\mu\}$) in (1) denotes a diagonal matrix of permeability μ.

Although (1) can be used to generate **H**-unknowns at any point along any direction, we have to keep in mind that they should be obtained at those locations and along those directions that can reversely generate desired **E**-unknowns in an accurate way. Hence, we choose the **H**-points, $\mathbf{r}_{hi}$, and the **H**-directions, $\hat{h}_i$, along a rectangular loop perpendicular to each **E**-unknown, and centering the **E**-unknown, as shown in Fig. 1. In this way, the resultant **H** fields can, in turn, generate **E** required in (1) accurately at the next time step, via the discretization of Ampere's law as follows:

$$\text{diag}\,(\{\epsilon\})\,\frac{\partial\{e\}}{\partial t} + \{j\} = \mathbf{S}_h\{h\} \tag{2}$$

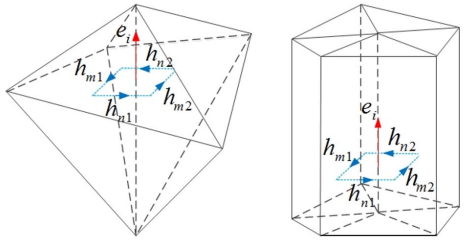

Fig. 1. Choice of **H** points and directions.

in which $\{j\}$ denotes a current source vector, $\mathbf{S}_h$ is a sparse matrix of size $N_e \times N_h$, representing a curl operation on **H**. Based on the **H** fields shown in Fig. 1, each row of $\mathbf{S}_h$ obviously has only four nonzero elements, whose column index corresponds to the global index of the four **H**-points associated with one **E**-unknown. In (2), the diag($\{\epsilon\}$) is a diagonal matrix of permittivity. From (1) and (2), we can also eliminate **H** and solve **E** as follows:

$$\text{diag}(\{\epsilon\})\frac{\partial^2\{e\}}{\partial t^2} + \mathbf{S}\{e\} = -\frac{\partial\{j\}}{\partial t} \tag{3}$$

where

$$\mathbf{S} = \mathbf{S}_h \text{diag}\left(\left\{\frac{1}{\mu}\right\}\right)\mathbf{S}_e. \tag{4}$$

When $\mathbf{S}_e = \mathbf{S}_h^T$, **S** is symmetrical and positive semidefinite, thus having nonnegative real eigenvalues only. Here, since the curl of **E** and the curl of **H** are carried out in a completely different fashion, $\mathbf{S}_e \neq \mathbf{S}_h^T$, and the resultant **S** is highly unsymmetrical.

B. Unsymmetrical FDTD Subgridding

In [28], an unsymmetrical FDTD subgridding method is developed, which utilizes the strength of an unsymmetrical discretization of curl operators in accuracy to build an accurate and flexible subgridding method. In this method, the final numerical system can also be cast into the form of (1) and (2), but with different $\mathbf{S}_e$ and $\mathbf{S}_h$ values.

In the method of [28], a row vector is generated for every patch in the grid, regardless of a 2-D or 3-D grid. This row vector represents a curl of **E** operation in the patch, which produces the time derivative of the normal **H** field at the patch center. This row vector is nothing but $\mathbf{S}_e^{(i)}$, the ith row of $\mathbf{S}_e$, and the row index corresponds to the patch index. A column vector, which is $\mathbf{S}_h^{(i)}$, is also generated for every patch in the grid. It represents how the normal **H** field at the patch center is used to generate the electric fields. The product of $\mathbf{S}_h^{(i)}$ and $\mathbf{S}_e^{(i)}$ makes a rank-1 matrix, the sum of which over all patches in the grid makes the total **S**. In a regular grid, $\mathbf{S}_e^{(i)}$ has only four nonzero elements, and $\mathbf{S}_h^{(i)} = (\mathbf{S}_e^{(i)})^T$. Hence, the symmetric and positive semidefiniteness of **S** is ensured. However, when the subgrids exist, as shown in [28], $\mathbf{S}_h^{(i)} = (\mathbf{S}_e^{(i)})^T$ is not satisfied.

C. General Unsymmetrical Systems Arising From Other Methods

The unsymmetrical system is also observed in many other methods, such as the nonorthogonal FDTD methods and other subgridding methods different from [28]. Although their ways of discretizing Maxwell's equations are different, and hence, the resultant $\mathbf{S}_e$ and $\mathbf{S}_h$ are different from those in the MFTD, they all can be cast into the format of (1) and (2). As long as the two curl operations are not made reciprocal of each other, which is the case to ensure the accuracy of the space discretization in a nonorthogonal grid or a grid with subgrids, the resultant numerical system is unsymmetrical.

In the second-order system where only one field unknown is solved, and in a single-mesh setup, such as that in the finite-element method, when the basis function for expanding the field unknown is different from the testing function, the resulting system matrix is also unsymmetrical.

The second-order system of equations for solving Maxwell's equations using various methods can be written into the following form:

$$\mathbf{D}_\epsilon \frac{\partial^2\{e\}}{\partial t^2} + \mathbf{S}\{e\} = b(t) \tag{5}$$

where $\mathbf{D}_\epsilon$ is associated with the permittivity, which can be either diagonal or nondiagonal, symmetric or unsymmetrical, depending on the method used for discretizing Maxwell's equations. **S** represents a discretized $\nabla\mu^{-1}\nabla\times$ operator. For an unsymmetrical treatment of the curl of **E** and the curl of **H**, **S** is unsymmetrical. Using different basis and testing functions, **S** is also unsymmetrical. Certainly, there exist other scenarios such as nonreciprocal materials, which can make **S** unsymmetrical as well.

D. Stability Analysis of an Unsymmetrical System

The time marching of (1) and (2) is usually performed in a leap-frog way, such as the one in the FDTD method. This is, in fact, equivalent to a central-difference-based explicit time marching of (3) or (5), which can be readily proved by eliminating one field unknown from the leap-frog-based time discretization of (1) and (2). Regardless of solving the first- or second-order systems, when $\mathbf{S} \neq \mathbf{S}^T$, such an explicit time marching is absolutely unstable. To see this clearly, we can discretize (5) using a central-difference-based explicit time marching and analyze its stability. The explicit discretization yields

$$\mathbf{D}_\epsilon(\{e\}^{n+1} - 2\{e\}^n + \{e\}^{n-1}) + \Delta t^2\mathbf{S}\{e\}^n = \Delta t^2\{b\}^n. \tag{6}$$

Removing the source term since it has nothing to do with the stability and performing a z transform of (6), we obtain

$$z^2 - (2 - \Delta t^2\lambda)z + 1 = 0 \tag{7}$$

where Δt is the time step and λ is the eigenvalue of $\mathbf{D}_\epsilon^{-1}\mathbf{S}$. If **S** is unsymmetrical, $\mathbf{D}_\epsilon^{-1}\mathbf{S}$ can have complex-valued and even negative eigenvalues. From (7), it can be seen that the two roots satisfy

$$|z_1 z_2| = 1. \tag{8}$$

Since neither $|z_1| = 1$ nor $|z_2| = 1$ is satisfied for complex λ, because

$$z_{1,2} = \frac{2 - \Delta t^2\lambda \pm \sqrt{\Delta t^2\lambda(\Delta t^2\lambda - 4)}}{2} \tag{9}$$

one of the roots must be greater than 1 in magnitude. In addition, if the eigenvalue is negative, one root must be out of the unit circle as well. As a result, the traditional explicit scheme for simulating an unsymmetrical system is absolutely unstable.

To overcome this stability problem, in [11]–[13], a backward-difference-based discretization of (5) is performed, which requires a lower bound of the time step for stability

$$\Delta t > \frac{2|\mathrm{Im}(\sqrt{\lambda})|}{|\sqrt{\lambda}|^2} \tag{10}$$

where $\mathrm{Im}(\cdot)$ denotes the imaginary part of $(\cdot)$. To avoid solving a matrix in time marching, a series expansion is used to derive an explicit inverse of the system matrix. $\{e\}$ at the $(n+1)$th time step is, hence, computed as

$$\{e\}^{n+1} = (\mathbf{I} - \tilde{\mathbf{M}} + \tilde{\mathbf{M}}^2 - \cdots + (-\tilde{\mathbf{M}})^k)\{f\} \tag{11}$$

where $\{f\} = 2\{e\}^n - \{e\}^{n-1} - \Delta t^2 \mathbf{D}_\epsilon^{-1} b^{n+1}$ and $\tilde{\mathbf{M}} = \Delta t^2 \mathbf{D}_\epsilon^{-1}\mathbf{S}$. For the series expansion to converge, an upper bound of the time step is imposed as follows:

$$\Delta t < \frac{1}{\sqrt{\rho(\mathbf{D}_\epsilon^{-1}\mathbf{S})}} \tag{12}$$

in which $\rho(\cdot)$ denotes the spectral radius, which is the largest eigenvalue magnitude. This time step is similar to the time step used in the Courant–Friedrichs–Lewy (CFL) condition. Hence, using the traditional explicit time step, one can use (11) to obtain a stable solution. However, such a series expansion with k terms requires k sparse matrix-vector multiplications. Although k is not large, which is, in general, no greater than 10, the resulting time marching is not as efficient as performing only one matrix-vector multiplication in the right-hand side, such as that in the traditional explicit FDTD method.

III. New Explicit Method for Simulating Unsymmetrical Systems With Guaranteed Stability

Based on the stability analysis in Section II-D, it appears that there is no way forward to make an explicit time marching stable for simulating an unsymmetrical system. However, we found the following explicit method worked out.

The method can be used to solve both the first-order Maxwell's equation and the second-order one in a stable fashion. Consider the first-order system. We discretize (1) in the following way:

$$\mathbf{S}_e(2\{e\}^n - \{e\}^{n-1}) = -\mathrm{diag}(\{\mu\})\frac{\{h\}^{n+\frac{1}{2}} - \{h\}^{n-\frac{1}{2}}}{\Delta t} \tag{13}$$

where we change $\{e\}^n$ after $\mathbf{S}_e$ used in the traditional explicit method to $2\{e\}^n - \{e\}^{n-1}$. Obviously, the discretization is explicit since we use the field solution at the previous time step to obtain the field at the current time step. As for the discretization of Ampere's law, we keep it the same as before and, hence, obtain

$$\mathbf{S}_h\{h\}^{n+\frac{1}{2}} = \mathrm{diag}(\{\epsilon\})\frac{\{e\}^{n+1} - \{e\}^n}{\Delta t} + \{j\}^{n+\frac{1}{2}} \tag{14}$$

where the time instants for $\{e\}$ and $\{h\}$, denoted by superscripts, are staggered by half.

Consider the second-order system shown in (5). We perform the following time discretization:

$$\mathbf{D}_\epsilon(\{e\}^{n+1} - 2\{e\}^n + \{e\}^{n-1}) + \Delta t^2 \mathbf{S}(2\{e\}^n - \{e\}^{n-1}) = \{f\}^n \tag{15}$$

where again $\{e\}^n$ after $\mathbf{S}$ used in the traditional explicit method is replaced by $\left(2\{e\}^n - \{e\}^{n-1}\right)$. In the MFTD, $\mathbf{D}_\epsilon = \mathrm{diag}\,(\{\epsilon\})$.

Now, if we carry out a stability analysis, we find a totally different result. Setting the excitation to be zero, as it is irrelevant to stability, and performing a z transform of (15), we obtain

$$z^2 - 2(1 - \Delta t^2\lambda)z + (1 - \Delta t^2\lambda) = 0 \tag{16}$$

where λ are the eigenvalues of $\mathbf{D}_\epsilon^{-1}\mathbf{S}$. Since $\mathbf{S}$ is unsymmetrical, λ can be either real or complex.

However, comparing (16) with (7), now, we have

$$|z_1 z_2| = |1 - \Delta t^2\lambda| \tag{17}$$

which is not 1 any more, and it can be made less than 1 via an appropriate choice of a time step. Hence, it becomes feasible now to make the magnitude of both roots less than 1, thus making the explicit time marching stable. In the following, we quantitatively derive a stability criterion for (15) and, thereby, (13) and (14).

Denoting $\Delta t^2\lambda$ by

$$\Delta t^2\lambda = a + jb \tag{18}$$

where a is the real part and b denotes the imaginary part as follows:

$$a = \Delta t^2 \mathrm{Re}(\lambda)$$
$$b = \Delta t^2 \mathrm{Im}(\lambda). \tag{19}$$

The two roots of (16) can be found as

$$z_1 = 1 - (a + jb) + \sqrt{-(a + jb) + (a + jb)^2} \tag{20}$$

$$z_2 = 1 - (a + jb) - \sqrt{-(a + jb) + (a + jb)^2}. \tag{21}$$

Let

$$\xi = -(a + jb) + (a + jb)^2 \tag{22}$$

which is

$$\xi = (a^2 - b^2 - a) + j(2a - 1)b. \tag{23}$$

Using the following property [29] of the square root of a complex number:

$$\sqrt{\xi} = \sqrt{\frac{|\xi| + \mathrm{Re}(\xi)}{2}} + \mathrm{sign}(\mathrm{Im}(\xi))\, j\sqrt{\frac{|\xi| - \mathrm{Re}(\xi)}{2}} \tag{24}$$

we obtain

$$z_{1,2} = 1 - (a + jb) \pm \left(\sqrt{\frac{|\xi| + \mathrm{Re}(\xi)}{2}} + \mathrm{sign}(\mathrm{Im}(\xi))\, j\sqrt{\frac{|\xi| - \mathrm{Re}(\xi)}{2}}\right). \tag{25}$$

If the product of the two roots is greater than 1 in magnitude, then at least one of the roots has a magnitude greater than 1. Therefore, to ensure stability, the following condition is necessary:

$$|z_1 z_2| = |1 - \Delta t^2 \lambda| = |1 - (a + jb)| < 1 \tag{26}$$

which results in

$$2a - a^2 - b^2 > 0. \tag{27}$$

Substituting (19) into it, we obtain

$$\Delta t < \sqrt{\frac{2\mathrm{Re}(\lambda)}{|\lambda|^2}} \tag{28}$$

which provides an upper bound for the choice of Δt.

$|z_1|^2$ can be evaluated as

$$\begin{aligned} |z_1|^2 = {} & 1 + 2(1-a)\sqrt{\frac{|\xi| + \mathrm{Re}(\xi)}{2}} \\ & - 2|b|\mathrm{sign}(2a-1)\sqrt{\frac{|\xi| - \mathrm{Re}(\xi)}{2}} \\ & + |\xi| - (2a - a^2 - b^2). \end{aligned} \tag{29}$$

In deriving (29), we utilize the fact that

$$\mathrm{sign}(\mathrm{Im}(\zeta)) = \mathrm{sign}(2a-1)\mathrm{sign}(b). \tag{30}$$

Similarly, we have

$$\begin{aligned} |z_2|^2 = {} & 1 - 2(1-a)\sqrt{\frac{|\xi| + \mathrm{Re}(\xi)}{2}} \\ & + 2|b|\mathrm{sign}(2a-1)\sqrt{\frac{|\xi| - \mathrm{Re}(\xi)}{2}} \\ & + |\xi| - (2a - a^2 - b^2). \end{aligned} \tag{31}$$

To ensure stability, $|z_1|^2 < 1$ and $|z_2|^2 < 1$ should be satisfied. Adding the two inequalities based on (29) and (31), we obtain the following condition:

$$|\xi| < 2a - a^2 - b^2 \tag{32}$$

which is clearly another necessary condition in addition to (27), and hence (28).

Since a is the product of the time step square and the real part of the eigenvalue as shown in (19), for a given time step, a can be an arbitrary nonnegative value. When $0 < a < 1/2$, clearly, between z_1 and z_2, z_1 has a larger magnitude because the two terms having the square roots are both positive. When $a > 1$, z_2 has a larger magnitude. For both cases, the largest magnitude square can be written as

$$\begin{aligned} |z|^2_{\max} = {} & 1 + \left(2|1-a|\sqrt{\frac{|\xi| + \mathrm{Re}(\xi)}{2}} + 2|b|\sqrt{\frac{|\xi| - \mathrm{Re}(\xi)}{2}}\right) \\ & + |\xi| - (2a - a^2 - b^2), \quad (0 < a < 1/2 \text{ or } a > 1). \end{aligned} \tag{33}$$

If we can prove that (33) is bounded by 1, then both roots are bounded by 1 in magnitude, and hence, the explicit simulation is stable. When $1/2 < a < 1$, the signs of the two square root terms in (29) and (31) are opposite to each other, and the magnitude square of the two roots can be written as follows:

$$\begin{aligned} |z|^2 = {} & 1 \pm \left(2|1-a|\sqrt{\frac{|\xi| + \mathrm{Re}(\xi)}{2}} - 2|b|\sqrt{\frac{|\xi| - \mathrm{Re}(\xi)}{2}}\right) \\ & + |\xi| - (2a - a^2 - b^2), \quad (1/2 < a < 1). \end{aligned} \tag{34}$$

Next, we derive the stability condition for all three cases of a.

A. For the Cases of $0 < a < 1/2$ and $a > 1$

To be stable, $|z|^2_{\max} < 1$. We, hence, obtain from (33) that

$$\begin{aligned} & \left(2|1-a|\sqrt{\frac{|\xi| + \mathrm{Re}(\xi)}{2}} + 2|b|\sqrt{\frac{|\xi| - \mathrm{Re}(\xi)}{2}}\right) \\ & \quad < -|\xi| + (2a - a^2 - b^2), \quad (0 < a < 1/2 \text{ or } a > 1). \end{aligned} \tag{35}$$

Since the left-hand side is positive, if the right-hand side is not positive, the above-mentioned condition can never be satisfied. However, as shown in (32), this condition is satisfied.

Performing a square operation on both the sides of (35) to remove the square roots, we obtain

$$\begin{aligned} & 4(1 - 2a + a^2)\frac{|\xi| + \mathrm{Re}(\xi)}{2} + 4b^2\frac{|\xi| - \mathrm{Re}(\xi)}{2} \\ & \quad + 8|1-a||b|\sqrt{\frac{|\xi|^2 - |\mathrm{Re}(\xi)|^2}{4}} \\ & \quad < 4a^2 - 4a|\xi| + |\xi|^2 + a^4 + b^4 + 2a^2b^2 \\ & \quad - 2(a^2 + b^2)(2a - |\xi|). \end{aligned} \tag{36}$$

Substituting

$$|\mathrm{Im}(\xi)| = \sqrt{|\xi|^2 - |\mathrm{Re}(\xi)|^2} \tag{37}$$

into (36), we have

$$\begin{aligned} & -|\xi|^2 + 2|\xi| + (2a^2 - 2b^2 - 4a + 2)\mathrm{Re}(\xi) \\ & \quad + 4|1-a||b||\mathrm{Im}(\xi)| \\ & \quad < a^4 + b^4 - 4a^3 - 4ab^2 + 2a^2b^2 + 4a^2. \end{aligned} \tag{38}$$

From (22), we obtain

$$|\xi|^2 = (a^2 - b^2 - a)^2 + b^2(2a-1)^2. \tag{39}$$

Substituting (39) into (38), we find

$$\begin{aligned} & 2|\xi| + 4|1-a||b||\mathrm{Im}(\xi)| \\ & \quad - 8a^2b^2 + a^2 - 3b^2 - 2a + 12ab^2 < 0. \end{aligned} \tag{40}$$

Since, now, the cases of $0 < a < 1/2$ and $a > 1$ are considered, for either of the cases, we have

$$4|1-a||b||\mathrm{Im}(\xi)| = -4b^2(1-a)(2a-1) \tag{41}$$

using which in (40), we obtain the following condition:

$$2|\xi| < 2a - a^2 - b^2. \tag{42}$$

Comparing (42) with (32), (42) is a more stringent condition. Hence, it overwrites the condition required in (32). This also means although (32) is necessary for stability, it is not sufficient.

B. For the Case of $1/2 < a < 1$

Since $|z|^2$ has the expression shown in (34) for this case, let both roots be bounded by 1, we obtain

$$\pm\left(2|1-a|\sqrt{\frac{|\xi|+\mathrm{Re}(\xi)}{2}}-2|b|\sqrt{\frac{|\xi|-\mathrm{Re}(\xi)}{2}}\right) < -|\xi|+(2a-a^2-b^2), \quad (\text{For } 1/2<a<1). \tag{43}$$

Since the right-hand side of (43) is positive ensured by (32), taking a square operation on both the sides of (43), we obtain

$$\left(2|1-a|\sqrt{\frac{|\xi|+\mathrm{Re}(\xi)}{2}}-2|b|\sqrt{\frac{|\xi|-\mathrm{Re}(\xi)}{2}}\right)^2 < (-|\xi|+(2a-a^2-b^2))^2, \quad (\text{For } 1/2<a<1). \tag{44}$$

Following a derivation similar to the other two cases, which are the steps from (36) to (40), we obtain the same inequality as (40) except that the term having $\mathrm{Im}(\xi)$ now becomes $-4|1-a||b||\mathrm{Im}(\xi)|$. This is equal to $-4b^2(1-a)(2a-1)$ as well since $1/2 < a < 1$. As a result, for all cases, (42) is the condition to be satisfied.

Taking a square on both the sides of (42), we obtain

$$3a^4+3b^4-4a^3+6a^2b^2-4ab^2+4b^2<0 \tag{45}$$

which can be expressed in terms of the real part and the imaginary part of λ as

$$3(|\mathrm{Re}(\lambda)|^2+|\mathrm{Im}(\lambda)|^2)^2\Delta t^4-4\mathrm{Re}(\lambda)(|(\mathrm{Re}(\lambda)|^2+|\mathrm{Im}(\lambda)|^2)\Delta t^2+4|\mathrm{Im}(\lambda)|^2<0. \tag{46}$$

The above-mentioned inequality can be readily solved, yielding the following condition:

$$\sqrt{\frac{2\mathrm{Re}(\lambda)-2\sqrt{|\mathrm{Re}(\lambda)|^2-3|\mathrm{Im}(\lambda)|^2}}{3|\lambda|^2}} < \Delta t < \sqrt{\frac{2\mathrm{Re}(\lambda)+2\sqrt{|\mathrm{Re}(\lambda)|^2-3|\mathrm{Im}(\lambda)|^2}}{3|\lambda|^2}}. \tag{47}$$

As can be seen, (47) provides a tighter upper bound, which overwrites the upper bound in (28). In addition, if $|\mathrm{Re}(\lambda)|^2 < 3|\mathrm{Im}(\lambda)|^2$, then no real-valued time step can be found to satisfy the above-mentioned condition, and hence, a time marching cannot be stable. Therefore, the following condition is required as well for stability:

$$|\mathrm{Im}(\lambda)| < \frac{|\mathrm{Re}(\lambda)|}{\sqrt{3}} \tag{48}$$

which is, in general, satisfied since the imaginary part of a complex eigenvalue is small compared with the real part if the method developed for solving Maxwell's equations is accurate. To summarize, (47) and (48) are the stability criteria of the proposed explicit time-domain method.

When the imaginary part is zero or negligible, the lower bound of (47) becomes zero, and thus, the condition is naturally satisfied. However, when the imaginary part of $\mathbf{S}$'s eigenvalues cannot be ignored, there is a lower bound on the time step. When the imaginary part does not exist or is negligible for the largest eigenvalue, the upper bound of (47) becomes

$$\Delta t < \sqrt{\frac{4}{3}}\frac{1}{\sqrt{\lambda_{\max}}} \tag{49}$$

where $\lambda_{\max}$ is the largest eigenvalue of $\mathbf{D}_\epsilon^{-1}\mathbf{S}$. This upper bound is, in fact, larger than (12). Hence, a larger time step is allowed in the proposed method compared with [11]. More importantly, this new time marching scheme is truly explicit. No series expansion is required. Hence, the proposed method is more efficient than the original MFTD method. Moreover, as can be seen from the aforementioned analysis, the proposed method is applicable to other unsymmetrical methods to make them stable since the curl operations represented by $\mathbf{S}_h$ and $\mathbf{S}_e$ in (13) and (14) and $\mathbf{S}$ in (15) can be arbitrary.

Accuracy Analysis of the Proposed Scheme: One may wonder why we made a choice of using $2\{e\}^n-\{e\}^{n-1}$ to replace $\{e\}^n$, and whether this choice is accurate or not, although it makes the time marching stable. In fact, $2\{e\}^n-\{e\}^{n-1}$ constitutes an accurate approximation of $\{e\}^{n+1}$, and $\{e\}^{n+1}$ is the value used in a backward difference scheme for discretizing the second-order wave equations, which is known to be accurate (see [3, Ch. 12]). To see this point clearly, if we replace $(2\{e\}^n-\{e\}^{n-1})$ by e^{n+1}, the left-hand side of (15) is nothing but a backward-difference-based discretization of (5). To derive it, we can perform a backward difference to discretize $(\partial e/\partial t)$ at the nth time instant, obtaining

$$\frac{\partial e}{\partial t}=\frac{e^n-e^{n-1}}{\Delta t} \tag{50}$$

upon which if we apply another backward difference, we obtain

$$\frac{\partial^2 e}{\partial t^2}=\frac{e^n-2e^{n-1}+e^{n-2}}{\Delta t^2}. \tag{51}$$

Using (51), we can write down a backward-difference-based discretization of (5) as follows:

$$\mathbf{D}_\epsilon\frac{e^n-2e^{n-1}+e^{n-2}}{\Delta t^2}+\Delta t^2\mathbf{S}e^n \tag{52}$$

for the nth time instant. Writing (52) for the $(n+1)$th time instant, we obtain

$$\mathbf{D}_\epsilon\frac{e^{n+1}-2e^n+e^{n-1}}{\Delta t^2}+\Delta t^2\mathbf{S}e^{n+1} \tag{53}$$

which is the same as shown in the left-hand side of (15) if e^{n+1} is replaced by $(2\{e\}^n-\{e\}^{n-1})$. The former (e^{n+1}) can be accurately approximated as the latter $((2\{e\}^n-\{e\}^{n-1}))$ because

$$\frac{\{e\}^n-\{e\}^{n-1}}{\Delta t}\approx\frac{\{e\}^{n+1}-\{e\}^n}{\Delta t} \tag{54}$$

that is, the slope in the nth segment is approximately equal to that in the $(n+1)$th segment. This is an accurate approximation since for a maximum frequency $f_{\max}$, the time step is generally chosen as $1/(10f_{\max})$ or even smaller so that the accuracy is satisfactory. In such a time interval or two time intervals, the field's temporal dependence can be well approximated by a linear function. Hence, the accuracy of (54) can be ensured and also controlled by the choice of time step.

TABLE I
ILLUSTRATION OF COMPLEX EIGENVALUES OF EXAMPLE A

	1	2	3	4
Real	5.15e+27	1.31e+28	2.26e+28	4.78e+28
Imaginary	±1.24e+25	±3.77e+25	±1.28e+26	±1.05e+27

The backward difference has been shown to be accurate in simulating an unsymmetrical system [11], [28], and the accuracy of the proposed explicit time marching is, thus, also ensured. In a general differencing scheme, a backward or forward difference appears to be less accurate than a central difference since it is first-order accurate, with a truncation accuracy of $O(\Delta t)$. However, each of the three difference schemes, in fact, produces the same result in a time interval where the field variation is at most a linear function. This is because they are all equal to the slope of the field line in the time interval. This is indeed the case in our time-domain simulations since the time step required by the sampling theorem is $1/(2f_{\max})$, while what is used in practice is $1/(10f_{\max})$ or even smaller for good accuracy. In such a time interval, a backward difference is also accurate.

IV. NUMERICAL RESULTS

In this section, we first demonstrate the performance of the proposed explicit MFTD for simulating unstructured meshes. A number of irregular meshes are simulated, and the accuracy and efficiency of the new method are compared with those of the original MFTD. We then apply the proposed explicit method to the recently developed unsymmetrical FDTD subgridding method [28] to make its explicit simulation stable. All simulations are carried out on an Intel Xeon CPU E5-2690 v2@3.00 GHz.

A. MFTD in a 2-D Irregular Triangular Mesh

The first example is a highly irregular 2-D mesh shown in Fig. 2(a), the size of which is 0.22 mm in the x-direction and 0.25 mm in the y-direction. The discretization results in 2081 edges and 1325 triangular patches. To investigate the accuracy of the proposed method in such a mesh, we set up a free-space wave propagation problem so that an analytical solution is available for comparison. The incident $\mathbf{E}$ is set to be $\mathbf{E} = \hat{y} f(t - x/c)$, where $f(t) = 2(t-t_0)\exp(-(t-t_0)^2/\tau^2)$, with $\tau = 2.0$ ps, $t_0 = 4\tau$, and c denotes the speed of light. This is also the total $\mathbf{E}$ in a free-space wave propagation problem. Specifically, since $\mathbf{E}$ is known, we impose an analytical boundary condition, i.e., the known value of tangential $\mathbf{E}$, on the outermost boundary of the mesh. We then numerically simulate the fields inside the mesh and correlate the results with the analytical solution.

Due to the highly irregular mesh, $\mathbf{S}$ is highly unsymmetrical, which has many complex eigenvalues whose imaginary parts are not as small as compared with the real parts. In Table I, we list some of the representative eigenvalues of $\mathbf{S}$. As can be seen, the imaginary part can be quite significant compared with the real part. Because of this, when we tried to perform a leap-frog scheme directly on the MFTD system of equations, the simulation immediately becomes unstable. Hence, a new explicit method like the proposed is necessary for simulating this example.

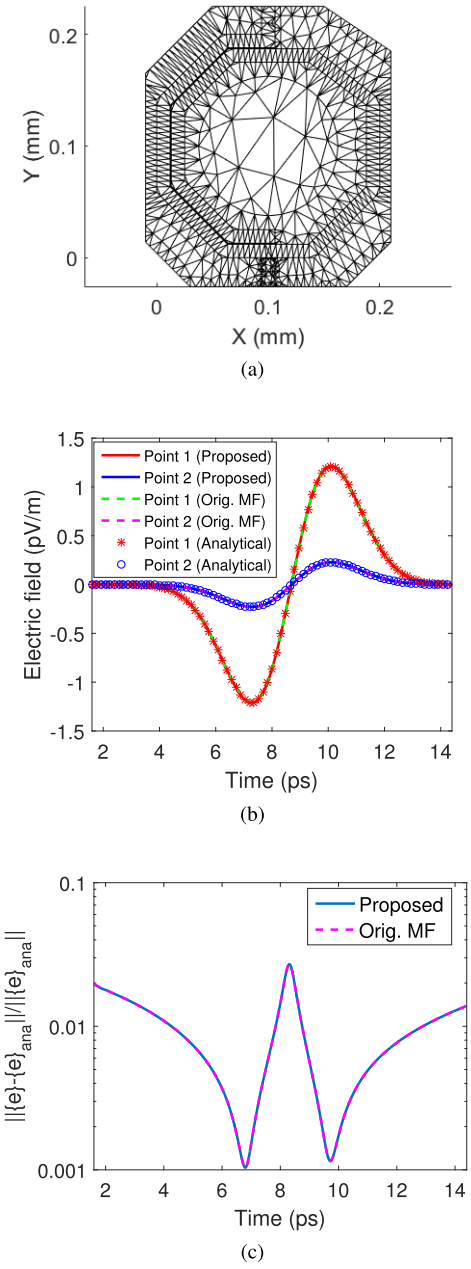

Fig. 2. Simulation of a 2-D triangular mesh. (a) Irregular triangular mesh. (b) Simulated two electric fields. (c) Entire $\mathbf{E}$-field solution error as a function of time.

The time step used in the proposed method is $\Delta t = 0.242$ fs, which is determined by (49). Note that the $\mathbf{S}$'s spectral radius can be analytically estimated from the smallest space step, and (49) has a good correlation with the CFL condition. In Fig. 2(b), we plot the electric fields of the 6811th and 6812th entries randomly selected from the unknown $\{e\}$ vector and compare them with the analytical solutions as well as those from the original MFTD method [11]. It can be clearly seen that the electric fields solved from the proposed method have excellent agreement with the analytical results and the results of [11]. To verify the accuracy everywhere in the computational domain, we evaluate the total solution error by

calculating $\|\{e\} - \{e\}_{\text{ana}}\|/\|\{e\}_{\text{ana}}\|$, where $\{e\}$ contains all e_i unknowns solved from the proposed method, and $\{e\}_{\text{ana}}$ is from the analytical solution. As can be seen from Fig. 2(b), the proposed method is not only accurate at the selected observation points as shown in Fig. 2(b) but also accurate at all other points. The center peak error in Fig. 2(c) is due to the comparison with close to zero fields. In addition, the error plot of the proposed method is on the top of that of the original MFTD method, and thus, the proposed method does not sacrifice the accuracy of the original scheme. Furthermore, it greatly shortens the CPU run time, as the method of [11] takes 88.05 s to finish the simulation, while the proposed method only costs 15.02 s.

B. MFTD in a 3-D Box Discretized Into Tetrahedral Mesh

The second example is a 3-D box discretized into tetrahedral elements, as shown in Fig. 3(a). The structure size is 1.0 m in the x-direction, 0.5 m in the y-direction, and 0.75 m in the z-direction. The discretization results in 544 edges and 350 elements. We also set up a free-space wave propagation problem in the given mesh to validate the accuracy of the proposed method against the analytical results. The incident **E** has the same form as that of the previous example, but with $\tau = 6.0$ ns in accordance with the new 3-D structure's dimension. The time step used in the proposed method is $\Delta t = 27.7$ ps, which is determined from (49). This also correlates well with the traditional CFL condition. In Fig. 3(b), we plot the electric fields of the 1st and 1832nd entries from the unknown $\{e\}$ vector and compare them with the analytical solutions and the method of [11]. Excellent agreement can be observed. We also plot the entire solution error shown in Fig. 3(c) versus time. It is evident that the proposed method is not only just accurate at certain points but also accurate at all points in the computational domain for all time instants simulated. The center peak in Fig. 3(c) is due to the comparison with close to zero fields. The proposed method takes 0.18 s only to finish the simulation without sacrificing accuracy, as can be seen from Fig. 3(c), while the method of [11] takes five times longer.

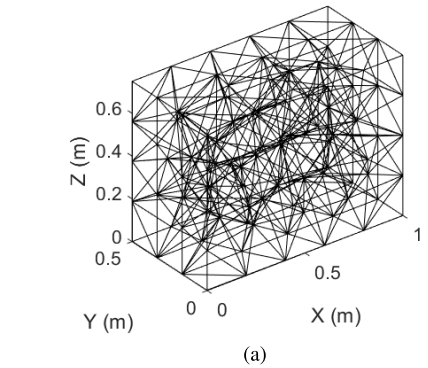

(a)

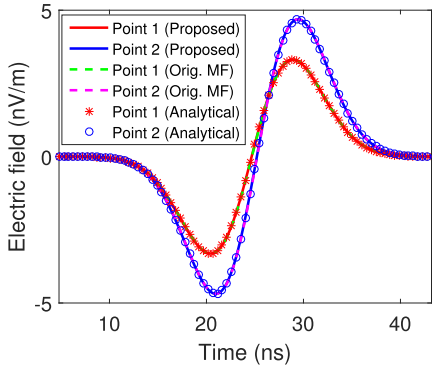

(b)

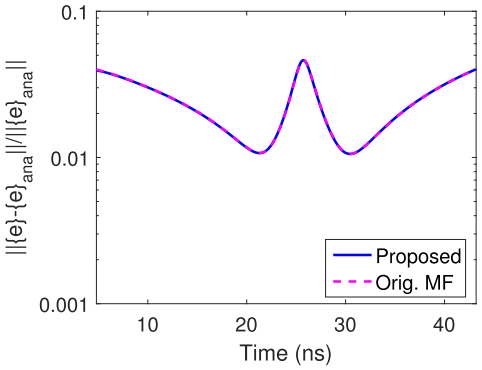

(c)

Fig. 3. Simulation of a 3-D box discretized into tetrahedral elements. (a) Tetrahedron mesh of a 3-D box. (b) Simulated two electric fields in comparison with the analytical results. (c) Entire **E**-field solution error as a function of time.

C. MFTD in a 3-D Sphere Discretized Into a Tetrahedral Mesh

The third MFTD example is a sphere discretized into tetrahedral elements in free space with a radius of 0.1 m, whose 3-D mesh is shown in Fig. 4(a). The discretization results in 3183 edges and 1987 tetrahedrons. The structure is illuminated by a plane wave having the same form as that in the first example but with $\tau = 2.0$ ns.

Similar to the previous examples, **S** is highly unsymmetrical having many complex eigenvalues. The imaginary part of some eigenvalues is even similar to the real part such as $9.672e21 \pm j1.923e21$. The traditional leap-frog scheme is found to be absolutely unstable in simulating this example no matter how the time step is chosen. The time step used in the proposed method is $\Delta t = 3.12$ ps, which is selected to satisfy (49). Two electric fields, whose indices in vector $\{e\}$ are 1 and 2942, respectively, are plotted in Fig. 4(b) in comparison with the analytical data. In Fig. 4(c), we plot the entire solution error versus time, where the accuracy of the proposed method is demonstrated.

We also simulate this example using the method in [11], whose $\Delta t = 2.70$ ps, which is restricted by (12). It takes 16.58 s to finish the simulation. In contrast, the proposed method only takes 3.37 s while achieving the same accuracy as can be seen from Fig. 4(c). The original number of time steps simulated with the proposed time marching scheme is 5132. We also simulate to a very late time where the number of time steps is more than 1 026 400. No late time instability is observed.

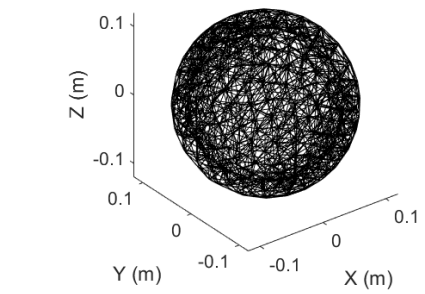

(a)

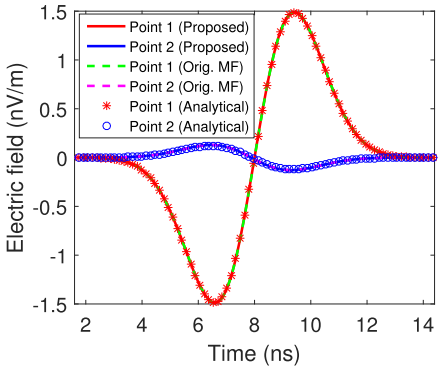

(b)

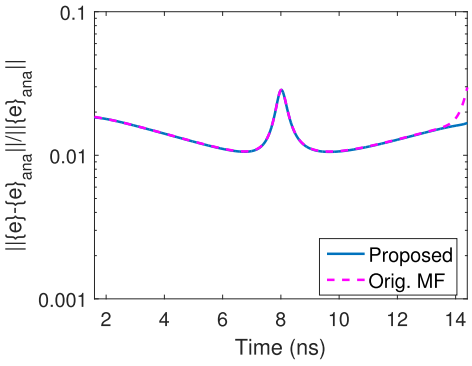

(c)

Fig. 4. Simulation of a 3-D sphere. (a) Tetrahedron mesh of a sphere. (b) Simulated two electric fields. (c) Entire **E**-field solution error as a function of time.

D. Unsymmetrical FDTD Subgridding: 2-D Grid With Multiple Subgrids

A 2-D wave propagation problem involving multiple subgrids is considered, whose space discretization is shown in Fig. 5(a). The size of the simulation domain in each direction is 1.0 m, the coarse grid size is $L_c = 0.1$ m, and the blue regions are subgrids where the grid ratio $L_c/L_f = 3$. $\mathbf{E}^{\text{inc}}$ is $\hat{y}2(t - t_0 - x/c)e^{(t-t_0-x/c)^2/\tau^2}$, $\tau = 20$ ns, and $t_0 = 4\tau$. All the boundaries are terminated by an exact absorbing boundary condition. The time step used is $\Delta t = 1/\sqrt{\|\mathbf{S}\|} = 44$ ps, which satisfies the stability criterion of the traditional explicit method. In Fig. 5(b), we plot the electric fields at the 1st and 340th entries in comparison with the analytical data. It can be seen that both the traditional explicit method, denoted by

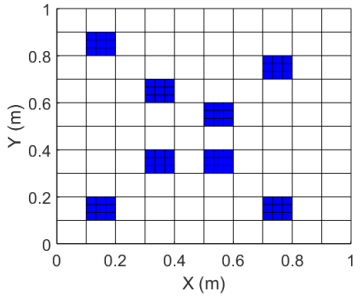

(a)

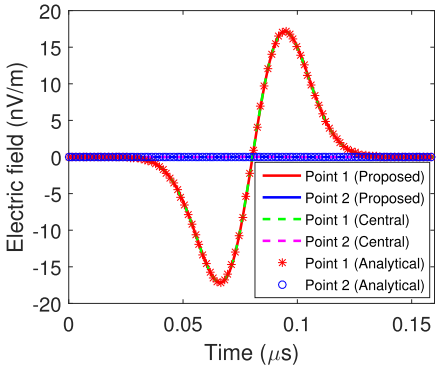

(b)

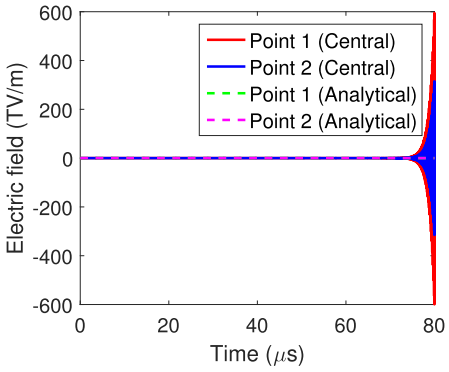

(c)

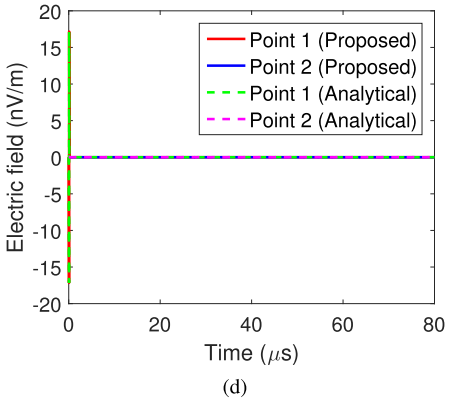

(d)

Fig. 5. Simulation of a 2-D subgridding problem. (a) Illustration of the grid. (b) Simulated two electric fields in comparison with the traditional explicit scheme and the analytical results. (c) Late time simulation using the traditional explicit scheme versus analytical results. (d) Late time simulation using the proposed method versus analytical results.

central in Fig. 5(b), and the proposed new explicit method generate accurate results.

However, when we elongate the time for simulation, the late time instability is observed from the traditional explicit time marching, as shown in Fig. 5(c). This is because of the existence of complex eigenvalues. For example, the 102th eigenvalue of the system matrix is found to be $1.5018e20 \pm 2.1538e16j$, making $|z| = 1.00004$. Although different from the MFTD, in the subgridding method, the imaginary part of the eigenvalue is smaller compared with the real part, as long as such a complex eigenvalue exists, the traditional explicit simulation cannot be made stable. The instability can be clearly observed when 1 818 000 time steps are simulated, using 68.58-s CPU time. In contrast, using the proposed explicit method and a similar CPU time of 69.57 s, no such instabilities are observed in the same late time simulation, which can be clearly seen from Fig. 5(d). After the early time response, the fields are stably simulated as zero in the late time.

E. Unsymmetrical FDTD Subgridding: 3-D Cube With Two Subgridding Cells

The second subgridding example is a free-space wave propagation problem in a 3-D cube. The size of the simulation domain in each direction is 1.0 m with a coarse grid size of $L_c = 0.1$ m. Two cells, which are centered at (0.15, 0.15, 0.15) and (0.45, 0.45, 0.45) m, respectively, are subdivided into fine grids with a grid ratio of $L_c/L_f = 3$. The base grid is shown with the blue subgrids in Fig. 6(a). We apply the same incident field and boundary condition as those in the previous example. The time step used is $\Delta t = 1/\sqrt{\|\mathbf{S}\|} = 35$ ps. In Fig. 6(b), we plot the electric fields at the 1st and 2694th entries versus the analytical data. It can be seen that both the proposed new explicit method and the traditional explicit method agree very well with the analytical solution. However, similar to the previous example, when we run the simulation to a late time, the traditional explicit method becomes unstable, as shown in Fig. 6(c), where the instability is observed after 1 142 750 time steps with a CPU time of 345.01 s. The complex eigenvalue pairs are observed from the unsymmetrical system matrix of the subgridding method. For example, the 965th eigenvalue is $5.4851e21 + 2.0377e16j$, making $|z| = 1.00005$. In contrast, despite the complex eigenvalues, using the proposed new method and a similar CPU time of 348.25 s, no such instabilities are observed in the late time, as can be seen from Fig. 6(d).

F. Inhomogeneous 3-D Phantom Head Beside a Wire Antenna

In this example, we simulate a large-scale phantom head beside a wire antenna [28], which involves many inhomogeneous materials. The size of the phantom head is $28.16 \times 28.16 \times 17.92$ cm. All the boundaries are truncated by the perfect magnetic conducting conditions. The wire antenna is located at $(3.52, 3.52, 2.52)$ cm, with a current pulse of $\hat{z}2(t - t_0)e^{-(t-t_0)^2/\tau^2}$ with $\tau = 0.5$ ns and $t_0 = 4\tau$. The base

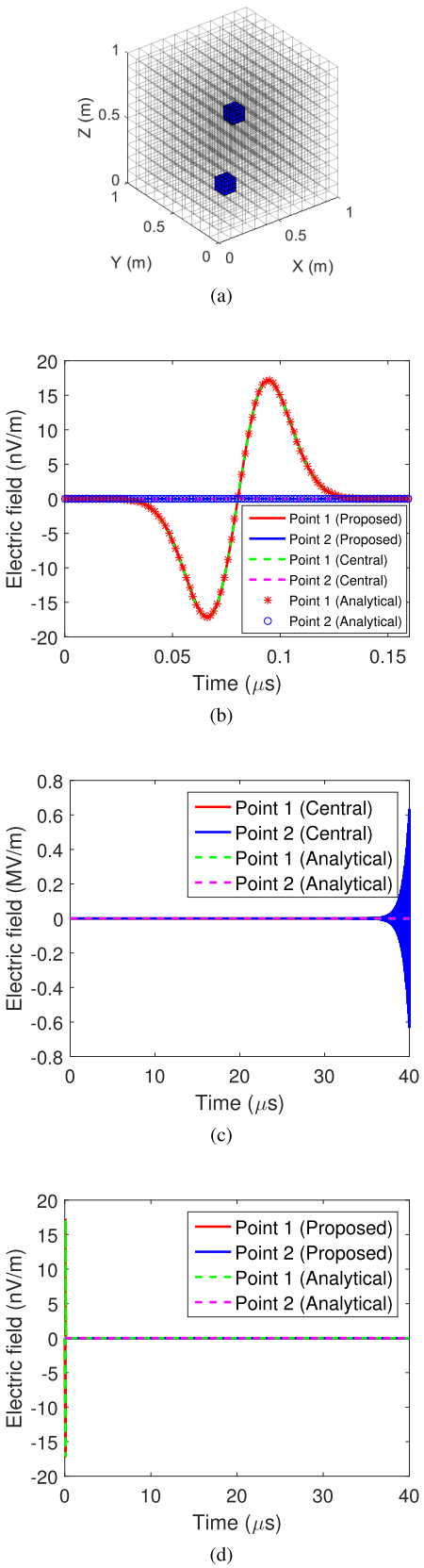

Fig. 6. Simulation of a 3-D subgridding problem. (a) Illustration of the grid. (b) Simulated two electric fields in comparison with the traditional explicit marching and analytical results. (c) Late time simulation using the traditional explicit marching versus analytical results. (d) Late time simulation using the proposed method versus analytical results.

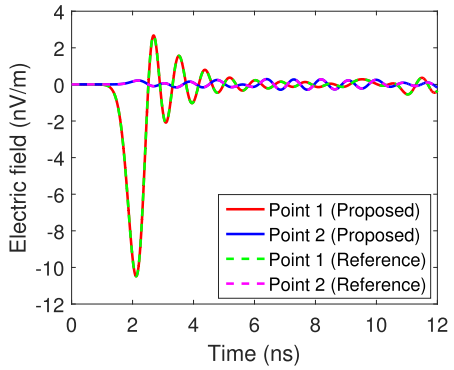

Fig. 7. Simulated electric field at two observation points in comparison with reference of a 3-D inhomogeneous problem.

grid size along the x-, y-, and z-directions is 4.4, 4.4, and 5.6 mm, respectively. To capture fine tissues, the base grid cell centered at $(14.3, 14.3, 9.24)$ cm is subdivided into subgrid cells in all directions with a grid ratio of 4, making that the subgrid grid size along the x-, y-, and z-directions is 1.1, 1.1, and 1.4 mm, respectively. We use the unsymmetrical subgridding method [28] as our reference with a time step of 1.1 ps. Due to the unsymmetrical property, the reference subgridding method [28] has to use (11) to obtain a stable solution with a series expansion of ten terms. In contrast, the proposed new method allows for a truly explicit time marching. In Fig. 7, the electric fields at two observation points whose locations are $(3.52, 3.52, 15.96)$ and $(24.64, 3.52, 15.96)$ cm are plotted in comparison with the reference results obtained using the same time step. It is clear that the two sets of results agree well. The unsymmetrical subgridding method [28] uses 1050.53 s to finish the simulation. In contrast, the proposed subgridding method only costs 539.03 s. The original number of time steps simulated with the proposed time marching scheme is 10 909. We also simulate to a very late time where the number of time steps is 1 090 900. No late time instability is observed.

V. Conclusion

In this article, we develop a truly explicit time marching scheme for solving unsymmetrical numerical systems in the time domain. The proposed method is theoretically proved to be stable despite the unsymmetrical system matrix. Meanwhile, the accuracy of the time marching is not sacrificed, and the time step size is not reduced. As a result, we make the MFTD method truly matrix-free, hence accentuating its advantage of having a diagonal mass matrix irrespective of the element shape used for discretization. We also successfully apply the proposed method to make the explicit time marching of an unsymmetrical FDTD subgridding method stable. Extensive numerical results are provided to demonstrate its validity and performance. The proposed method is generic, and hence, it can be used in the other unsymmetrical methods to guarantee their stability in an explicit time-domain simulation.

References

[1] K. Yee, "Numerical solution of initial boundary value problems involving Maxwell's equations in isotropic media," *IEEE Trans. Antennas Propag.*, vol. AP-14, no. 3, pp. 302–307, May 1966.

[2] A. Taflove and S. C. Hagness, *Computational Electrodynamics: The Finite-Difference Time-Domain Method*. Boston, MA, USA: Artech House, 2000.

[3] J.-M. Jin, *The Finite Element Method in Electromagnetics*. New York, NY, USA: Wiley, 2002.

[4] R. A. Chilton and R. Lee, "Conservative and provably stable FDTD subgridding," *IEEE Trans. Antennas Propag.*, vol. 55, no. 9, pp. 2537–2549, Sep. 2007.

[5] A. Van Londersele, D. De Zutter, and D. V. Ginste, "A new hybrid implicit–explicit FDTD method for local subgridding in multiscale 2-D TE scattering problems," *IEEE Trans. Antennas Propag.*, vol. 64, no. 8, pp. 3509–3520, Aug. 2016.

[6] F. Bekmambetova, X. Zhang, and P. Triverio, "A dissipation theory for three-dimensional FDTD with application to stability analysis and subgridding," *IEEE Trans. Antennas Propag.*, vol. 66, no. 12, pp. 7156–7170, Dec. 2018.

[7] M. R. Cabello *et al.*, "A hybrid Crank–Nicolson FDTD subgridding boundary condition for lossy thin-layer modeling," *IEEE Trans. Microw. Theory Techn.*, vol. 65, no. 5, pp. 1397–1406, May 2017.

[8] L. Codecasa, B. Kapidani, R. Specogna, and F. Trevisan, "Novel FDTD technique over tetrahedral grids for conductive media," *IEEE Trans. Antennas Propag.*, vol. 66, no. 10, pp. 5387–5396, Oct. 2018.

[9] M. Abbaszadeh and M. Dehghan, "The two-grid interpolating element free Galerkin (TG-IEFG) method for solving Rosenau-regularized long wave (RRLW) equation with error analysis," *Appl. Anal.*, vol. 97, no. 7, pp. 1129–1153, 2018.

[10] M. Movahhedi, A. Abdipour, A. Nentchev, M. Dehghan, and S. Selberherr, "Alternating-direction implicit formulation of the finite-element time-domain method," *IEEE Trans. Microw. Theory Techn.*, vol. 55, no. 6, pp. 1322–1331, Jun. 2007.

[11] J. Yan and D. Jiao, "Accurate and stable matrix-free time-domain method in 3-D unstructured meshes for general electromagnetic analysis," *IEEE Trans. Microw. Theory Techn.*, vol. 63, no. 12, pp. 4201–4214, Dec. 2015.

[12] J. Yan and D. Jiao, "Matrix-free time-domain method for general electromagnetic analysis in 3-D unstructured meshes—Modified-basis formulation," *IEEE Trans. Microw. Theory Techn.*, vol. 64, no. 8, pp. 2371–2382, Aug. 2016.

[13] J. Yan and D. Jiao, "Time-domain method having a naturally diagonal mass matrix independent of element shape for general electromagnetic analysis—2-D formulations," *IEEE Trans. Antennas Propag.*, vol. 65, no. 3, pp. 1202–1214, Mar. 2017.

[14] K. Zeng and D. Jiao, "Matrix-free method for transient Maxwell-thermal cosimulation in arbitrary unstructured meshes," *IEEE Trans. Microw. Theory Techn.*, vol. 66, no. 12, pp. 5439–5448, Dec. 2018.

[15] R. Holland, "Finite-difference solution of Maxwell's equations in generalized nonorthogonal coordinates," *IEEE Trans. Nucl. Sci.*, vol. NS-30, no. 6, pp. 4589–4593, Dec. 1983.

[16] M. Fusco, "FDTD algorithm in curvilinear coordinates (EM scattering)," *IEEE Trans. Antennas Propag.*, vol. 38, no. 1, pp. 76–89, Jan. 1990.

[17] J.-F. Lee, R. Palandech, and R. Mittra, "Modeling three-dimensional discontinuities in waveguides using nonorthogonal FDTD algorithm," *IEEE Trans. Microw. Theory Techn.*, vol. 40, no. 2, pp. 346–352, Feb. 1992.

[18] N. K. Madsen, "Divergence preserving discrete surface integral methods for Maxwell's curl equations using non-orthogonal unstructured grids," *J. Comput. Phys.*, vol. 119, no. 1, pp. 34–45, Jun. 1995.

[19] C. H. Chan, J. T. Elson, and H. Sangani, "An explicit finite-difference time-domain method using Whitney elements," presented at the IEEE Int. Symp. Antennas Propag., Jun. 1994, pp. 1768–1771.

[20] S. Gedney, F. S. Lansing, and D. L. Rascoe, "Full wave analysis of microwave monolithic circuit devices using a generalized Yee-algorithm based on an unstructured grid," *IEEE Trans. Microw. Theory Techn.*, vol. 44, no. 8, pp. 1393–1400, Aug. 1996.

[21] C. F. Lee, B. J. McCartin, R. T. Shin, and J. A. Kong, "A triangular-grid finite-difference time-domain method for electromagnetic scattering problems," *J. Electromagn. Waves Appl.*, vol. 8, no. 4, pp. 449–470, Aug. 1994.

[22] M. Hano and T. Itoh, "Three-dimensional time-domain method for solving Maxwell's equations based on circumcenters of elements," *IEEE Trans. Magn.*, vol. 32, no. 3, pp. 946–949, May 1996.

[23] J. A. Roden, "Broadband electromagnetic analysis of complex structures with the finite-difference time-domain techniques in general curvilinear coordinates," Ph.D. dissertation, Dept. Elect. Eng., Univ. Kentucky, Lexington, KY, USA, 1997.

[24] S. D. Gedney and J. A. Roden, "Numerical stability of nonorthogonal FDTD methods," *IEEE Trans. Antennas Propag.*, vol. 48, no. 2, pp. 231–239, Feb. 2000.
[25] P. Thoma and T. Weiland, "A consistent subgridding scheme for the finite difference time domain method," *Int. J. Numer. Model., Electron. Netw., Devices Fields*, vol. 9, no. 5, pp. 359–374, Sep. 1996.
[26] O. Podebrad, M. Clemens, and T. Weiland, "New flexible subgridding scheme for the finite integration technique," *IEEE Trans. Magn.*, vol. 39, no. 3, pp. 1662–1665, May 2003.
[27] L. Kulas and M. Mrozowski, "Reciprocity principle for stable subgridding in the finite difference time domain method," presented at the Int. Conf. 'Comput. Tool' (EUROCON), Sep. 2007, pp. 106–111.
[28] J. Yan and D. Jiao, "An unsymmetric FDTD subgridding algorithm with unconditional stability," *IEEE Trans. Antennas Propag.*, vol. 66, no. 8, pp. 4137–4150, Aug. 2018.
[29] M. Abramowitz and I. A. Stegun, *Handbook of Mathematical Functions with Formulas, Graphs, and Mathematical Tables*. New York, NY, USA: Dover, 1964.
[30] K. Zeng and D. Jiao, "Explicit matrix-free time-domain method in unstructured meshes," in *IEEE MTT-S Int. Microw. Symp. Dig.*, Boston, MA, USA, Jun. 2019, pp. 132–135, Paper Tu2B-7.

Kaiyuan Zeng (S'13–M'19) received the B.S. degree in electronic engineering and information science from the University of Science and Technology of China, Hefei, China, in 2012, and the Ph.D. degree in electrical engineering from Purdue University, West Lafayette, IN, USA, in 2019.

He is currently with Intel Corporation, Chandler, AZ, USA. His current research interests include signal and power integrity analysis, RF design, and computational electromagnetics.

Dr. Zeng was a recipient of the Honorable Mention Award of the IEEE International Symposium on Antennas and Propagation in 2018 and the Best Student Paper Award from the IEEE Wireless and Microwave Technology Conference in 2015.

Dan Jiao (M'02–SM'06–F'16) received the Ph.D. degree in electrical engineering from the University of Illinois at Urbana–Champaign, Champaign, IL, USA, in 2001.

She was with the Technology Computer-Aided Design (CAD) Division, Intel Corporation, until September 2005, as a Senior CAD Engineer, a Staff Engineer, and a Senior Staff Engineer. In September 2005, she joined Purdue University, West Lafayette, IN, USA, as an Assistant Professor with the School of Electrical and Computer Engineering, where she is currently a Professor. She has authored three book chapters and over 260 articles in refereed journals and international conferences. Her current research interests include computational electromagnetics, high-frequency digital, analog, mixed-signal, and RF integrated circuit (IC) design and analysis, high-performance VLSI CAD, modeling of microscale and nanoscale circuits, applied electromagnetics, fast and high-capacity numerical methods, fast time-domain analysis, scattering and antenna analysis, RF, microwave, and millimeter-wave circuits, wireless communication, and bioelectromagnetics.

Dr. Jiao received the 2013 S. A. Schelkunoff Prize Paper Award from the IEEE Antennas and Propagation Society, which recognizes the best paper published in the IEEE TRANSACTIONS ON ANTENNAS AND PROPAGATION during the previous year. She was among the 21 women faculty selected across the country as the 2014–2015 Fellow of Executive Leadership in Academic Technology and Engineering (ELATE) at Drexel, a national leadership program for women in the academic STEM fields. She has been named a University Faculty Scholar by Purdue University since 2013. She was among the 85 engineers selected throughout the nation for the National Academy of Engineering's 2011 U.S. Frontiers of Engineering Symposium. She was a recipient of the 2010 Ruth and Joel Spira Outstanding Teaching Award, the 2008 National Science Foundation (NSF) CAREER Award, the 2006 Jack and Cathie Kozik Faculty Start-up Award (which recognizes an outstanding new faculty member of the School of Electrical and Computer Engineering, Purdue University), the 2006 Office of Naval Research (ONR) Award under the Young Investigator Program, the 2004 Best Paper Award presented at the Intel Corporation's annual corporate-wide technology conference (Design and Test Technology Conference) for her work on generic broadband model of high-speed circuits, the 2003 Intel Corporations Logic Technology Development (LTD) Divisional Achievement Award, the Intel Corporations Technology CAD Divisional Achievement Award, the 2002 Intel Corporations Components Research the Intel Hero Award (Intel-wide she was the tenth recipient), the Intel Corporation's LTD Team Quality Award, and the 2000 Raj Mittra Outstanding Research Award presented by the University of Illinois at Urbana–Champaign. She has served as a reviewer for many IEEE journals and conferences. She is an Associate Editor of the IEEE TRANSACTIONS ON COMPONENTS, PACKAGING, AND MANUFACTURING TECHNOLOGY and the IEEE JOURNAL ON MULTISCALE AND MULTIPHYSICS COMPUTATIONAL TECHNIQUES.